Journal of Materials Chemistry C

ROYAL SOCIETY OF CHEMISTRY

PAPER

View Article Online
View Journal

Cite this: DOI: 10.1039/d6tc00388e

A significant impact of nitrogen substitution on the solid-state electronic structure: a case of 1,3,6,8-tetrakis(methylchalcogeno)-2,7-diazapyrene

Kirill Bulgarevich *[a] and Kazuo Takimiya *[abc]

Nitrogen substitution of carbon atoms in polycyclic aromatic hydrocarbons is a promising approach to develop novel π-conjugated molecules, preserving a similar molecular shape and isoelectronic structure, both of which are key to maintaining a solid-state electronic structure that governs optoelectronic properties. We report here the synthesis and characterization of 1,3,6,8-tetrakis(methylthio)-2,7-diazapyrene (MT-azapyrene), together with its selenium analogue, 1,3,6,8-tetrakis(methylseleno)-2,7-diazapyrene (MS-azapyrene), an isoelectronic homologue of the ultrahigh-mobility organic semiconductor, 1,3,6,8-tetrakis(methylthio)pyrene (MT-pyrene). For the synthesis of MT- and MS-azapyrene, we have newly developed 1,3,6,8-tetrachloro-2,7-diazapyrene, which was then utilized in a nucleophilic aromatic substitution reaction with methylthiolate and methylselenolate anions. Single-crystal X-ray analysis revealed the molecular and crystal structures of MT- and MS-azapyrene; to our surprise, their crystal structures were characterized as one-dimensional inclined brickwork structures, markedly different from the two-dimensional brickwork structures of the pyrene counterparts, despite the similarity in molecular shape between the pyrene and azapyrene derivatives. Because of the difference in the crystal structures, the carrier mobility of MT- and MS-azapyrene was far lower, 0.30 $cm^2 V^{-1} s^{-1}$ and 0.40 $cm^2 V^{-1} s^{-1}$ (on average), respectively, than that of MT-pyrene (>30 $cm^2 V^{-1} s^{-1}$). These results demonstrate that even subtle structural changes, such as nitrogen substitution, alter the crystal structure and thus drastically alter transport properties.

Received 5th February 2026,
Accepted 31st March 2026

DOI: 10.1039/d6tc00388e

rsc.li/materials-c

Introduction

In the development of optoelectronic materials based on π-conjugated systems, such as polycyclic aromatic hydrocarbons (PAHs), controlling the molecular electronic structure is key to tuning the energy levels of frontier molecular orbitals and the optical bandgap.[1] Heteroatom substitution of carbon atoms in PAH frameworks is one of the promising molecular modifications.[2–4] Among them, the substitution of carbon atoms with nitrogen atoms is a prevailing approach,[5–7] as it preserves the isoelectronic structures and similar molecular shapes after the substitution. Maintaining similar molecular shapes is often crucial for preserving a similar packing structure in the solid state, which in turn determines the solid-state electronic structure. This is well-exemplified by the nitrogen-embedded derivatives of 6,13-bis(triisopropylsilylethynyl)-pentacene (TIPS-pentacene),[8,9] *e.g.*, 6,13-bis((triisopropylsilyl)-ethynyl)-5,7,12,14-tetraazapentacene (TIPS-TAP), which has a similar brickwork (BW) crystal structure to that of TIPS-pentacene, and one of the TIPS-TAP derivatives with the BW crystal structure showed an impressive ultrahigh mobility of up to 28 $cm^2 V^{-1} s^{-1}$.[10]

1,3,6,8-Tetrakis(methylthio)pyrene (MT-pyrene, Fig. 1a) is one of the best molecular semiconductors, showing an ultrahigh mobility (>30 $cm^2 V^{-1} s^{-1}$) and band-like transport properties.[11] Such superior electronic properties are endorsed by its two-dimensional (2D) electronic structure in the solid state, thanks to the BW crystal structure.[12] However, molecules similar to MT-pyrene, such as 2,5,8,11-tetrakis(methylthio)-perylene (MT-perylene),[13] 1,3,6,8-tetrakis(methylseleno)pyrene (MS-pyrene),[14] 1,4,7,10-tetrakis(methylthio)coronene (MT-coronene),[15] and 1,3,5,7-tetrakis(methylthio)dibenzo[*cd*,*gh*][2,5]-diselenapentalene (MT-DBDSP),[16] crystallized into a structure slightly different from that of MT-pyrene. The subtle changes in molecular arrangement in the crystal structures did not ensure efficient molecular orbital overlap and/or the formation of a 2D electronic structure in the solid state, resulting in rather

[a] *RIKEN Center for Emergent Matter Science (CEMS), 2-1 Hirosawa, Wako, Saitama 351-0198, Japan. E-mail: takimiya@riken.jp*
[b] *Tohoku University Advanced Institute for Materials Research (AIMR), 2-1-1 Katahira, Aoba-ku, Sendai, Miyagi 980-8577, Japan*
[c] *Department of Chemistry, Graduate School of Science, Tohoku University, 6-3 Aoba, Aramaki, Aoba-ku, Sendai, Miyagi 980-8578, Japan*

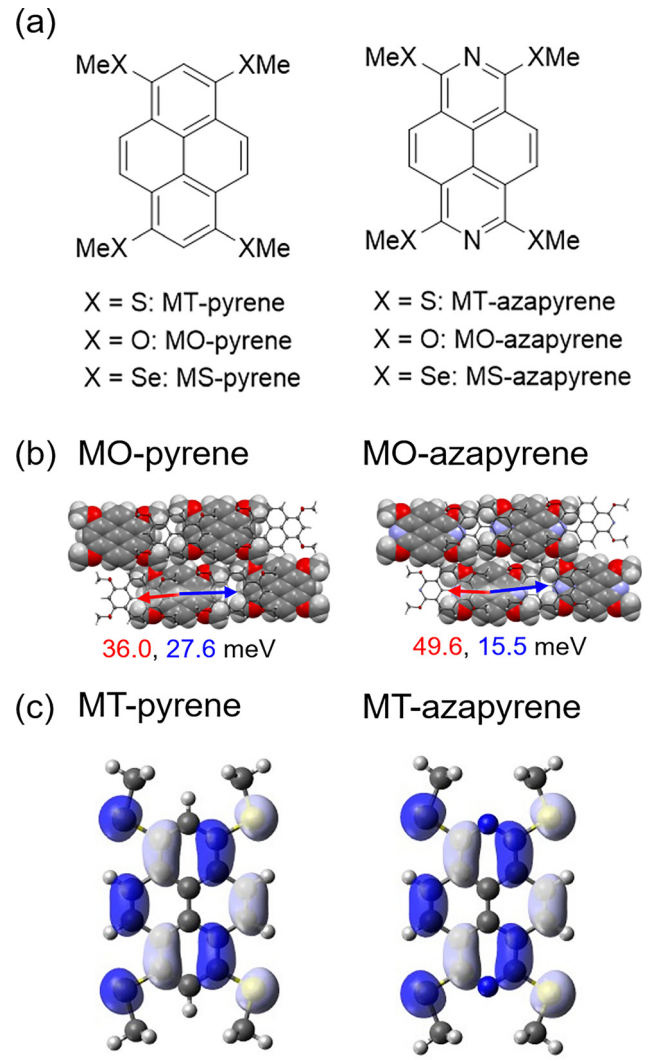

Fig. 1 (a) Molecular structures of methylchalcogenolated pyrenes and azapyrenes. (b) Crystal structures of MO-azapyrene and MO-pyrene with transfer integral values in the π-stacking layer indicated. (c) Distribution of the HOMO of MT-pyrene and MT-azapyrene.

poor transport properties.[17] The only two examples that retain similar electronic structures to MT-pyrene[11] are 1,3,8,10-tetrakis(methylthio)peropyrene (MT-peropyrene)[18] and 1,3,6,8-tetramethoxypyrene (MO-pyrene, Fig. 1),[14] the former of which showed an ultrahigh mobility of up to 30 $cm^2 V^{-1} s^{-1}$ in the SC-FETs. The latter molecule, MO-pyrene, on the other hand, despite its isostructural nature with MT-pyrene, exhibited inferior transport properties compared to MT-pyrene, owing to the methoxy group with an oxygen atom, which is not well-suited for enhancing intermolecular orbital overlap.

Recently, Miyake *et al.* reported the synthesis and crystal structure of 1,3,6,8-tetramethoxy-2,7-diazapyrene (MO-azapyrene, Fig. 1a), which is isostructural with MO-pyrene, with similar crystallographic parameters (Fig. 1b).[19,20] The solid-state electronic structures and transport properties (Fig. S1) were also similar to those of MO-pyrene,[14] strongly implying that the perturbation from the nitrogen atom in the azapyrene core should be negligible in solid-state electronic structures (Fig. 1b). These considerations prompted us to examine the methylthiolated 2,7-diazapyrene derivative, namely, 1,3,6,8-tetrakis(methylthio)-2,7-diazapyrene (MT-azapyrene, Fig. 1a), which possesses an isoelectronic structure with MT-pyrene (Fig. 1c), as a candidate for another ultrahigh-mobility molecular semiconductor. Here, we describe the synthesis and characterization of MT-azapyrene and its selenium analogue, methylselenolated azapyrene (MS-azapyrene, Fig. 1a), *via* the corresponding tetrachlorinated azapyrene.

Experimental

Synthesis

1,2-Bis(2,6-dichloro-5-methylpyridin-3-yl)ethene (**3**): a solution of 3-bromomethyl-2,6-dichloro-5-methylpyridine (**2**, 5.33 g, 21 mmol) in toluene (*ca.* 20 mL) was concentrated under reduced pressure to remove residual water. The residue was placed under vacuum, back-filled with argon, and redissolved in dry tetrahydrofuran (THF, 50 mL). The solution was cooled to −78 °C using a dry-ice/hexane bath, and a 26% (w/w) solution of lithium bis(trimethylsilyl)amide (LiHMDS) in THF (17 mL, 22 mmol) was added dropwise over 10 min, maintaining the internal temperature below −55 °C. After stirring for 15 min at −78 °C, the cooling bath was removed, and the reaction mixture was allowed to warm to room temperature. The mixture was poured into water (*ca.* 100 mL) and extracted with dichloromethane (3 × 200 mL). The combined organic layers were concentrated under reduced pressure, affording a colorless crystalline solid. The solid was collected from the flask using methanol, filtered, washed with acetone, and dried under vacuum to give compound **3** (3.00 g, 83%).

^{1}H NMR ($CDCl_3$, 400 MHz): δ 7.87 (s, 2H), 7.30 (s, 2H), 2.437 (s, 3H), 2.436 (s, 3H). ^{13}C NMR ($CDCl_3$, 100 MHz): δ 149.7, 146.1, 137.7, 132.1, 129.8, 126.6, 19.1. HRMS (APCI) *m*/*z*: $[M]^+$ calcd for $C_{14}H_{10}{}^{35}Cl_4N_2$ 345.9593; found 345.9592.

2,4,7,9-Tetrachloro-1,10-dimethyl-3,8-phenanthroline (**4**): a solution of compound **3** (1.02 g, 2.9 mmol) and iodine (0.20 g, 0.80 mmol) in toluene (1.3 L) was irradiated with a high-pressure mercury lamp while air was bubbled through the mixture for 2 h. After irradiation, the reaction mixture was extracted with aqueous sodium sulfite solution to remove residual iodine, and the organic layer was concentrated under reduced pressure. The resulting solid was collected from the flask using methanol, filtered, washed successively with water and acetone, and dried under vacuum to afford compound **4** as a yellow solid (0.87 g, 86%).

^{1}H NMR ($CDCl_3$, 400 MHz): δ 8.15 (s, 2H), 2.52 (s, 6H). ^{13}C NMR ($CDCl_3$, 100 MHz): δ 147.9, 146.9, 137.4, 128.9, 127.1, 125.2, 21.3. HRMS (APCI) *m*/*z*: $[M]^+$ calcd for $C_{14}H_8{}^{35}Cl_4N_2$: 343.9436; found 343.9418.

1,10-Bis(bromomethyl)-2,4,7,9-tetrachloro-3,8-phenanthroline (**5**): carbon tetrachloride (50 mL) was degassed by bubbling argon through the solvent for 20 min. Compound **4** (1.25 g, 3.6 mmol), azobisisobutyronitrile (AIBN, 0.023 g, 0.14 mmol), and *N*-bromosuccinimide (NBS, 1.77 g, 9.9 mmol)

were then added. The reaction mixture was refluxed under a nitrogen atmosphere for 16 h. After cooling to room temperature, the mixture was poured into water (*ca.* 100 mL) and extracted with dichloromethane (2 × 200 mL). The combined organic layers were concentrated under reduced pressure. The resulting yellow-green crystalline solid was collected from the flask using methanol, filtered, washed with methanol, and dried under vacuum to give compound **5** (0.92 g, 51%).

^{1}H NMR ($CDCl_3$, 400 MHz): δ 8.28 (s, 2H), 5.06 (d, J = 10.6 Hz, 2H), 4.86 (d, J = 10.6 Hz, 2H). ^{13}C NMR ($CDCl_3$, 100 MHz): δ 150.3, 149.0, 133.6, 127.7, 127.4, 126.0, 27.5. HRMS (APCI) m/z: $[M]^+$ calcd for $C_{14}H_6{}^{79}Br_2{}^{35}Cl_4N_2$ 499.7646; found 499.7645.

1,3,6,8-Tetrachloro-2,7-diazapyrene (**1c**): compound **5** (0.67 g, 1.3 mmol) was placed in a dry flask, which was sealed, evacuated, and back-filled with argon. Dry tetrahydrofuran (THF, 100 mL) was added, and the solution was cooled to −78 °C using a dry-ice/hexane bath. In a separate flask, also sealed, evacuated, and back-filled with argon, THF (50 mL) was added and cooled to −78 °C, followed by the addition of LiHMDS (26 w/w% solution in THF, 2.3 mL, 3.0 mmol). The solution of **5** was then added dropwise to the LiHMDS solution over 10 min. The combined solution was stirred for an additional 15 min at −78 °C and then allowed to warm to room temperature. The reaction mixture was poured into water and extracted with dichloromethane (3 × 100 mL), and the combined organic layers were concentrated under reduced pressure. The resulting solid was collected from the flask using methanol, filtered, washed with acetone, and dried under vacuum to afford compound **1c** as a green-yellow solid (0.34 g, 75%).

^{1}H NMR (TCE-d_2, 400 MHz, 130 °C): δ 8.54 (s, 4H) ^{13}C NMR (TCE-d_2, 100 MHz, 130 °C): δ 144.6, 129.5, 125.8, 123.9. HRMS (APCI) m/z: $[M]^+$ calcd for $C_{14}H_4{}^{35}Cl_4N_2$ 339.9129; found 339.9139.

1,3,6,8-Tetrakis(methylthio)-2,7-diazapyrene (MT-azapyrene): a dry flask was charged with compound **1c** (0.20 g, 0.59 mmol) and dry *N*,*N*-dimethylformamide (DMF, 30 mL). Methyl 3-(methylthio)propionate (0.6 mL, 5 mmol) and potassium *tert*-butoxide (*t*BuOK, 0.55 g, 5 mmol) were added under a flow of nitrogen. The reaction mixture was stirred at 100 °C for 16 h. After cooling to room temperature, the mixture was poured into water (*ca.* 100 mL), and the resulting precipitate was collected by filtration, washed successively with methanol and acetone, and dried under vacuum to give MT-azapyrene (0.15 g, 65%) as a dark brown solid.

A portion of the product (85 mg) was purified by sublimation to afford yellow needle-shaped crystals, which were further purified by sequential hot solvent washing (methanol, hexane, and acetone), followed by hot extraction with xylene and two additional rounds of sublimation, yielding a device-grade material (32 mg).

^{1}H NMR (TCE-d_2, 400 MHz, 120 °C): δ 8.07 (s, 4H), 2.92 (s, 12H) ^{13}C NMR (TCE-d_2, 100 MHz, 120 °C): δ 152.3, 121.8, 121.1, 120.2, 13.2. HRMS (APCI) m/z: $[M]^+$ calcd for $C_{18}H_{16}N_2S_4$ 388.0191; found 388.0183.

1,3,6,8-Tetrakis(methylseleno)-2,7-diazapyrene (MS-azapyrene): a dry flask was charged with compound **1c** (0.10 g, 0.30 mmol) and dry *N*,*N*-dimethylformamide (DMF, 20 mL). Methyl 3-(methylseleno)propionate (0.30 mL) and potassium *tert*-butoxide (*t*BuOK, 0.20 g, 1.8 mmol) were added under a flow of nitrogen. The reaction mixture was stirred at 100 °C for 16 h. After cooling to room temperature, the mixture was poured into water (*ca.* 100 mL), and the resulting precipitate was collected by filtration, washed successively with methanol and acetone, and dried under vacuum to give MS-azapyrene (0.088 g, 51%) as a dark brown solid.

A portion of the product (63 mg) was purified by sublimation to afford orange needle-shaped crystals, which were further purified by sequential hot solvent washing (methanol, hexane, and acetone), followed by hot extraction with xylene and two additional rounds of sublimation to give a device-grade material (20 mg).

Due to the limited solubility of MS-azapyrene, no meaningful ^{13}C NMR spectrum could be acquired even in TCE-d_2 at 130 °C.

^{1}H NMR (TCE-d_2, 400 MHz, 100 °C): δ 8.02 (s, 4H), 2.81 (s, 12H). HRMS (APCI) m/z: $[M]^+$ calcd for $C_{18}H_{16}N_2{}^{76}Se_4$ 563.8077; found 563.8091.

Crystal growth and single-crystal X-ray analysis

Single crystals for single-crystal X-ray analysis and single-crystal FETs were grown by microspacing sublimation under a nitrogen atmosphere (2 mm gap, 30 min), using heater temperatures of 320 °C and 340 °C for MT- and MS-azapyrene, respectively.[21]

Single-crystal X-ray analyses were carried out on a Rigaku Oxford Diffraction XtaLAB Synergy Custom DW system with a HyPix-6000HE detector (CuKα radiation, wavelength: 1.5418 Å, multilayer confocal optics). The structures were solved using the SHELXT program.[22] Non-hydrogen atoms were refined anisotropically.[23] All calculations were carried out by using the crystallographic software package Olex2 (ver. 1.5.0).[24] The crystal data are summarized in the SI (Tables S1–S3).

Single-crystal field-effect transistors

Heavily doped n-type Si wafers with thermally grown SiO_2 layers (200 nm) were cleaned by sonication in acetone for 10 min twice, followed by ultraviolet-ozone treatment for more than 30 min. CYTOP (AGC, 3 wt%) solution in CT-SOLV180 (AGC) was spin-coated on the wafer at 3000 rpm for 1 min, and the wafer was dried at 180 °C on a hot plate in the air.[25] The thickness of the CYTOP film (∼90 nm) was measured using AFM (NanoNavi IIs/NanoCute), and the wafer with the CYTOP layer was used as the substrate for the device fabrication. On top of the substrate, the thin crystals (*ca.* 100 nm) were laminated by hand, and the source and drain electrodes were defined by painting colloidal graphite (EM Science). The SC-FET devices were evaluated under ambient conditions.

Theoretical calculations

Molecular geometry optimization was carried out using the Gaussian16 program package.[26] Reorganization energy (λ) of the molecules was calculated by using the adiabatic potential energy surface method using the Gaussian16 program package. Intermolecular electronic coupling (transfer integral, V) in

different molecular dimers extracted from the single-crystal structures was calculated using the Amsterdam Density Functional (ADF) program.[27] With λ_s and V_s known, anisotropic theoretical mobilities were calculated in accordance with the literature.[28]

Results and discussion

Synthesis using 1,3,6,8-tetrachloro-2,7-diazapyrene

2,7-Diazapyrene derivatives have recently been focused on as potential optoelectronic materials,[19,20,29,30] and thus, various methods for the synthesis of a range of derivatives have been developed. For the synthesis of MT-azapyrene, 1,3,6,8-tetrafunctionalized 2,7-diazapyrenes, such as tetrapivaloxy (**1a**, Scheme 1a)[19] and tetratriflato[29] derivatives (**1b**, Scheme 1a), seem to be the potential precursors. The former proved unsuitable as a substrate for the substitution reaction with methylthio groups, either *via* aromatic nucleophilic substitution or *via* catalytic coupling reaction with a tin sulfide reagent (see the SI). On the other hand, for the synthesis of the tetratriflato derivative (**1b**), potassium graphite, a key reducing agent, is required and is not readily available in our laboratory. Additionally, for practical reasons in our laboratory environments (stability and handling in air), the halogenated derivatives, such as 1,3,6,8-tetrachloro-2,7-diazapyrene (**1c**), were considered the optimal precursors for MT-azapyrene.

We thus designed a synthesis route to **1c** from a functionalized pyridine derivative, 3-bromomethyl-2,6-dichloro-5-methylpyridine (**2**),[31,32] which was readily synthesized by the Diels–Alder reaction of 3,5-dichloro-2*H*-1,4-oxazin-2-one with propargyl bromide (Scheme 1b). Compound **2** was first treated with lithium hexamethyldisilazide (LiHMDS)[33] to afford *trans*-1,2-bis(2,6-dichloro-5-methylpyridin-3-yl)ethene (**3**), which was then cyclized into the tetrachlorodiazaphenanthrene derivative (**4**).[34] After the bromination of the methyl groups to give the corresponding bis(bromomethyl)diazaphenanthrene derivative (**5**), the second LiHMDS treatment gave the desired **1c** as a stable and less soluble crystalline solid. **1c** was found to be a particularly stable intermediate, showing clean weight loss without residual decomposition in TG analysis (Fig. S7a).

The introduction of methylthio groups was finally accomplished by a nucleophilic aromatic substitution reaction, using an *in situ*-generated methylthiolate anion derived from commercially available methyl 3-methylthiopropionate and potassium *tert*-butoxide.[14] Similarly, the methylseleno derivative (MS-azapyrene) was synthesized by treating **1c** with methyl 3-methylselenopropionate[14] with potassium *tert*-butoxide. Note that MT- and MS-azapyrene are remarkably stable and decompose less than the corresponding pyrene analogs in TG analysis (Fig. S7b).

Compared to the one-pot synthesis of **1a** and **1b** from naphthalene tetracarboxylic diimide,[19,20,29] the present multistep synthesis of **1c** has drawbacks, but the ease of handling and amenability to the introduction of the sulfur- (and selenium-) based functional groups could make **1c** a useful alternative reactive intermediate for various 1,3,6,8-substituted 2,7-diazapyrene derivatives.

Crystal structures and single-crystal field-effect transistors (SC-FETs) of MT- and MS-azapyrene

The crystal structures of MT- and MS-azapyrene are depicted in Fig. 2, along with their corresponding pyrene derivatives. The crystallographic data are summarized in Tables S1 and S2. As already mentioned, MO-azapyrene and MO-pyrene are isostructural to each other (Fig. 1b);[20] however, to our surprise, the crystal structures of MT- and MS-azapyrene are significantly different from those of the pyrene derivatives. The crystal structures of MT- and MS-azapyrene belong to the $P\bar{1}$ space group, with two half-molecules in the asymmetric unit ($Z = 2$), and are classified as inclined brickwork (iBW) structures. The structures are similar to those of one of the polymorphs of MT-peropyrene (also $P\bar{1}$ with $Z = 2$).[35] A similar iBW structure was also observed in one of the polymorphs of MS-pyrene, although with a different space group ($P2_1/n$, Fig. 2).[14] Crystallographic measurements performed under varied temperatures indicate similar volumetric thermal expansion for MT- and MS-azapyrene ($\sim 1.3 \times 10^{-4}$ Å^3 K^{-1}), which is typical of organic

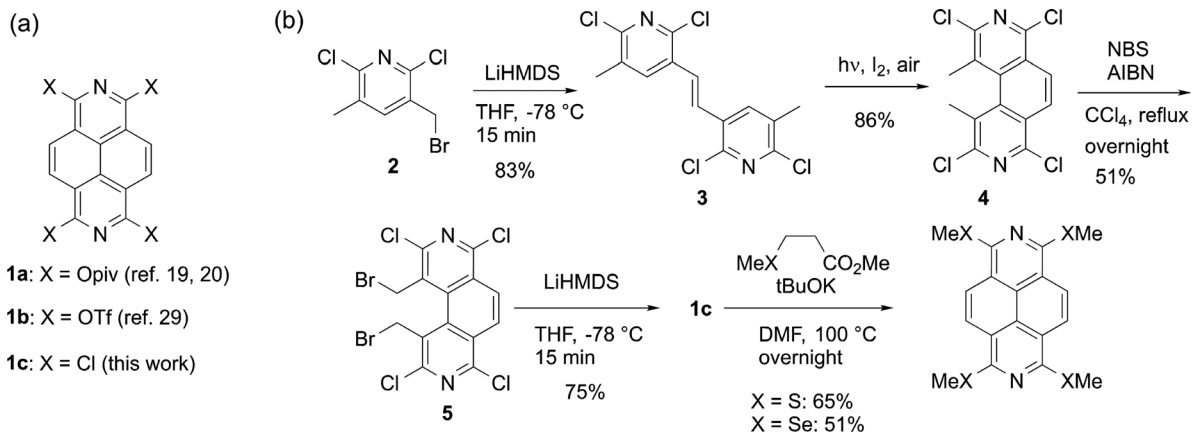

Scheme 1 (a) Potential precursors of MT- and MS-azapyrene. (b) Synthesis of MT- and MS-azapyrene *via* the corresponding 1,3,6,8-tetrachloro derivative (**1c**).

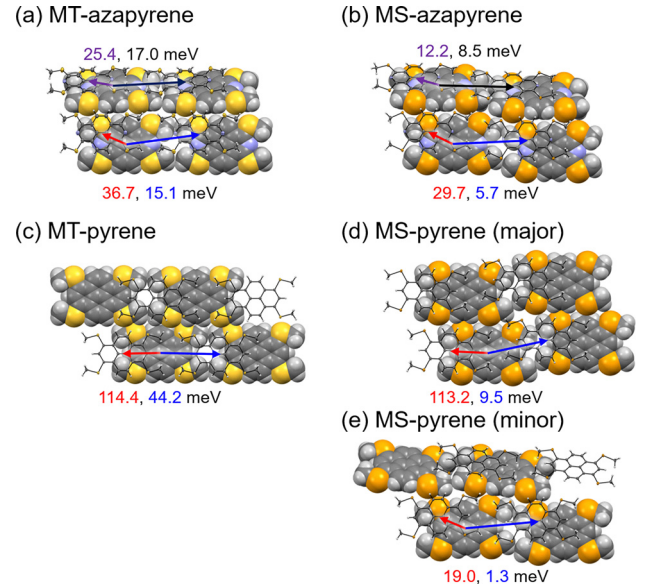

Fig. 2 Crystal structures of MT/MS-azapyrenes (a) and (b) and the corresponding MT/MS-pyrenes (c)–(e). MS-pyrene has two polymorphs: major (d) and minor (e). Transfer integrals in two π-stacking directions are indicated by red and blue arrows with corresponding values. The additional non-equivalent π-stacking directions in MT/MS-azapyrenes (a) and (b) are indicated by purple and black arrows with corresponding values.

molecular crystals dominated by weak intermolecular interactions. The expansion is slightly anisotropic, with the smallest change observed along the *c*-axis.

This structural divergence directly affects intermolecular electronic coupling (transfer integral) in the solid state. Because the $P\bar{1}$ structures with $Z = 2$ contain two crystallographically non-equivalent π-stacking layers, the intermolecular transfer integrals of HOMO were evaluated for all non-equivalent π-stacking molecular pairs (Fig. 2a and b).[27] For MT-azapyrene, the major (minor) π-stacking directions exhibit transfer integrals of 36.7 and 25.4 meV (15.4 and 17.0 meV). These values are considerably lower than those in the crystal structure of MT-pyrene (114 and 44.2 meV)[11] and are somewhat similar to other iBW polymorphs observed in the methylchalcogenated series, such as the minor polymorph of MS-pyrene (19.0 and 1.3 meV).[14] The characteristic feature of the iBW structures observed in these compounds is that one of the π-stacking molecules dominates the overlap area of the π-stacking layer, *i.e.*, one-dimensional (1D) structure, but at the same time, there is a significant offset in the molecular short-axis direction, which significantly decreases intermolecular orbital overlap, despite the large overlap area (Fig. 2).[15] The crystal structure of MS-azapyrene is virtually identical to that of MT-azapyrene with similarly low values of the transfer integrals in the π-stacking layers: 29.7 and 12.2 meV for the major π-stacking direction and 5.7 and 8.5 meV for the minor π-stacking direction.

Photoelectron yield spectroscopy measurements gave ionization potentials of 5.40 and 5.45 eV for MT- and MS-azapyrene, respectively, indicating that the HOMO levels remain within a suitable range for p-type OFET operation (Fig. S4). The UV-vis absorption spectra show similar absorption maxima for the azapyrene derivatives (λ_{max} = 446 and 449 nm for MT- and MS-azapyrene, respectively) with optical band gaps of 2.61 and 2.62 eV (Fig. S5), confirming that the electronic structures of the azapyrene derivatives remain close to those of the corresponding pyrene analogues despite the incorporation of nitrogen atoms into the π-core and the substantial differences in their crystal packing (Fig. S6, Table S4).[14]

To evaluate how these structural changes manifest in device performance, we fabricated single-crystal FETs (SC-FETs) using MT- and MS-azapyrene crystals grown by microspacing sublimation under atmospheric pressure.[21] The crystals were laminated onto CYTOP-coated (90 nm thick) SiO_2/Si substrates (total gate dielectric capacitance of 8.9 nF cm^{-2}),[25] and the source-drain electrodes were painted on the crystal ends with water-based colloidal graphite, resulting in the bottom-gate/top-contact FETs. The devices were evaluated in the air. The out-of-plane X-ray diffraction of the SC-FETs confirmed that all diffraction peaks correspond to the *b*- and *c*-axes out-of-plane orientations of the iBW structures, indicating no polymorphism in both compounds (Fig. S8). Fig. 3a and b represent the output (top) and transfer (middle) characteristics of MT- and MS-azapyrene SC-OFETs, respectively, measured at gate (V_g) and drain (V_d) voltages of up to −30 V. The devices showed nearly ideal characteristics with almost no hysteresis for both compounds, but the carrier mobility was low: 0.30 ± 0.07 cm^2 V^{-1} s^{-1} and 0.40 ± 0.08 cm^2 V^{-1} s^{-1} for MT- and MS-azapyrene, respectively (10 and 7 devices, respectively). Based on the hopping model with transfer integrals (Fig. 2) and reorganization energies of 220 and 183 meV, respectively, the theoretical mobilities for MT- and MS-azapyrene were estimated as 0.27 and 0.32 cm^2 V^{-1} s^{-1}, respectively (Fig. 3a and b, bottom, Fig. S9).[28] Temperature-dependent measurements of the SC-FET devices further support the hopping transport mechanism. For both MT- and MS-azapyrene, the mobility decreased with decreasing temperature in the 320–230 K range. Arrhenius analysis yielded activation energies of 0.070 eV for MT-azapyrene and 0.033 eV for MS-azapyrene (Fig. S10), which are consistent with thermally activated hopping transport. These results indicate that methylchalcogenated azapyrene derivatives are far less promising as organic semiconductors than their corresponding pyrene derivatives, primarily because of their iBW structures in the solid state.

Estimation of the cause of the crystal structure change

A similar crystal-structure change from the BW structure has been observed in MT-pyrene-related molecules, even in isoelectronic structures, *e.g.*, MS-pyrene and MT-DBDSP. In these selenium-containing molecules, the molecular shapes are fairly affected by the incorporated selenium atoms. For example, with long C–Se bonds in the methylseleno groups in MS-pyrene, the space between the two methylseleno groups at 1,3- and 6,8-positions is slightly larger than that in MT-pyrene, and to avoid void formation in the crystal structure, the displacement along the short molecular axis effectively fills the space.[14] On the other hand, the MT-DBDSP molecule has three chalcogen

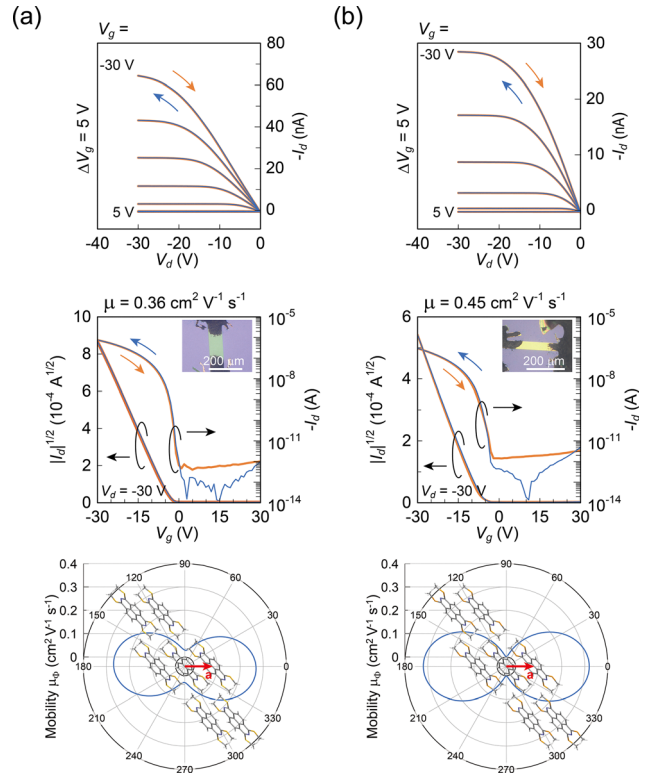

Fig. 3 Output (top) and transfer (middle) characteristics and simulated anisotropic mobility based on the hopping model of MT- (a) and MS- (b) azapyrene. The bottom plot was generated using the transfer integral values of 36.7 and 15.4 meV for MT-azapyrene and 29.7 and 5.7 meV for MS-azapyrene.

atoms on each side of the molecule, *i.e.*, two sulfur atoms from the methylthio groups and the core selenium atom, which causes steric congestion at the edges of the molecule, leading to a displacement along the short molecular axis.[16] In the present azapyrene case, however, the molecular shape is almost identical to that of the pyrene counterpart (Fig. S2), suggesting that a simple steric/shape-based origin is unlikely.

Recently, the different crystal structures of organic semiconducting molecules have been rationalized by the intermolecular quadrupole interactions,[36–39] and, thus, we also examined this scheme to explain the crystal structure change (Table S5). However, no clear differences were identified that could account for the observed change in packing motifs.

To probe a possible electronic driving force, we examined the atomic partial charges of the isolated molecules calculated using the Gaussian program at the B3LYP/6-31G(d) level (Fig. 4). The charge distributions are very similar in the pyrene and azapyrene series for each methylchalcogeno derivative. The notable difference is the charge of the nitrogen atom (0.3 units more negative) compared to the corresponding carbon atom at the 2-position of the pyrene core. In the crystal structure of MT-pyrene, the π-stacking layer features an almost complete overlap of the carbon atom at the 2-position of one molecule with the corresponding carbon atom of a neighboring molecule (Fig. 2). Such a configuration can be disfavored in MT- and MS-azapyrene because the corresponding position is occupied by a nitrogen atom with a large negative partial charge, which would increase electrostatic repulsion.

The present charge distribution analysis also explains why MO-azapyrene preserves the brickwork packing motif similar to that of MO-pyrene. The oxygen atom in the methoxy substituent carries a substantial negative charge (approximately −0.5), while sulfur and selenium atoms are weakly positive and nearly neutral, respectively. As a consequence, only in the MO derivatives, the oxygen atoms, regardless of the core atom at the 2-position, form an array of negatively charged sites along the molecular short axis (Fig. 4). This arrangement of atomic charge favors a packing motif in which the negatively charged array is aligned with the relatively positive central region of a neighboring molecule, resulting in very similar packing structures for MO-pyrene and MO-azapyrene, despite the presence of the ring nitrogen atom.

The present analysis indicates that the introduction of strongly polarizable heteroatoms, such as nitrogen atoms in the core or oxygen atoms in the substituents, can modify local electrostatic interactions and thereby alter the preferred packing structure even when the overall molecular shape and electronic structure remain largely unchanged. These insights provide a useful perspective for crystal structure design by controlling heteroatom placement and local charge distribution in molecular structures.

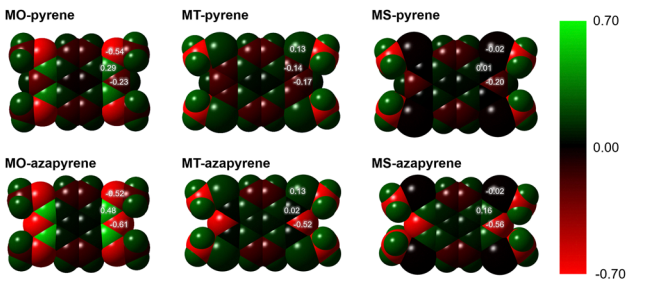

Fig. 4 Substituent- and core-dependence of atomic partial charges calculated for MX-pyrene and MX-azapyrene derivatives (Gaussian; B3LYP/6-31G(d)). The labels highlight the representative charges on the heteroatoms (O, S, and Se), the *ipso* carbon bonded to the substituent, and the core atom at the 2-position (corresponding to the nitrogen substitution position in azapyrene). The color scale ranges from red (negative potential) to green (positive potential), in atomic units.

Conclusions

A practical multistep route to 1,3,6,8-tetrakis(methylthio)-2,7-diazapyrene (MT-azapyrene) and its selenium analogue (MS-azapyrene) *via* the halogenated precursor 1,3,6,8-tetrachloro-2,7-diazapyrene (**1c**) was developed. Despite the stepwise synthesis, compared to previously reported azapyrene derivatives with reactive functional groups at the 1, 3, 6, and 8 positions, **1c** is remarkably stable, easy to handle in air, and highly reactive toward aromatic nucleophilic substitution reactions, making it a valuable and general intermediate for the preparation of functionalized azapyrene derivatives.

Single-crystal X-ray analysis revealed that both MT- and MS-azapyrene crystallize into iBW structures, which are distinct

from the 2D BW structures of MT-pyrene and MO-azapyrene, despite their similar molecular and electronic structures. As a consequence of adopting the 1D iBW structure with small orbital overlaps, MT- and MS-azapyrene exhibited low carrier mobilities (0.30 ± 0.07 and 0.40 ± 0.08 $cm^2 V^{-1} s^{-1}$, respectively). These results demonstrate that even such subtle nitrogen substitution drastically alters the crystal structure and thus transport properties.

To understand the significant crystal-structure change caused by nitrogen substitution of MT- and MS-pyrene, we focused on atomic partial charges, which suggest that the local charge distribution in molecular structures can cause crystal-structure changes. We thus hope that the insights emerging from the present work on azapyrene derivatives will deepen the molecular design strategy to improve crystal packing in the solid state and further enhance transport properties.

Author contributions

All experimental work, including synthesis, characterization, X-ray crystallographic analyses, theoretical calculations, and the fabrication/evaluation of SC-FETs, was performed by K. B. and K. T. K. B. and K. T. designed the target compounds and the synthetic scheme, supervised the experiments, and conducted data analyses. K. T. and K. B. directed the project. The draft manuscript was written by K. B. and K. T., and all authors finalized it through proofreading. All authors approved the final version of the manuscript.

Conflicts of interest

There are no conflicts to declare.

Data availability

The data supporting this article have been included as part of the supplementary information (SI). Supplementary information: experimental and characterization data, including crystallographic data and NMR and HRMS spectra. See DOI: https://doi.org/10.1039/d6tc00388e.

The experimental and analytical methods described in the paper are available from the corresponding authors upon reasonable request.

CCDC 2528768–2528778 contain the supplementary crystallographic data for this paper.[40a–k]

Acknowledgements

This work was financially supported by JSPS KAKENHI (Grant Numbers JP20H05865, JP23H00307, JP24KK0113, and JP25K07839). We gratefully acknowledge the Supercomputer System at the Advanced Center for Computing and Communication (ACCC) of RIKEN and the Center for Computational Materials Science, Institute for Materials Research, Tohoku University for the use of MASAMUNE-IMR (MAterials science Supercomputing system for Advanced MUlti-scale simulations towards NExt-generation-Institute for Materials Research) for theoretical calculations. Elemental analyses were carried out at the Molecular Structure Characterization Unit, RIKEN Center for Sustainable Resource Science (CSRS).

Notes and references

1 V. Coropceanu, J. Cornil, D. A. da Silva Filho, Y. Olivier, R. Silbey and J.-L. Brédas, Charge Transport in Organic Semiconductors, *Chem. Rev.*, 2007, **107**, 926–952.
2 K. Takimiya, S. Shinamura, I. Osaka and E. Miyazaki, Thienoacene-based organic semiconductors, *Adv. Mater.*, 2011, **23**, 4347–4370.
3 A. Borissov, Y. K. Maurya, L. Moshniaha, W.-S. Wong, M. Żyła-Karwowska and M. Stępień, Recent Advances in Heterocyclic Nanographenes and Other Polycyclic Heteroaromatic Compounds, *Chem. Rev.*, 2022, **122**, 565–788.
4 M. Hirai, N. Tanaka, M. Sakai and S. Yamaguchi, Structurally Constrained Boron-, Nitrogen-, Silicon-, and Phosphorus-Centered Polycyclic π-Conjugated Systems, *Chem. Rev.*, 2019, **119**, 8291–8331.
5 H. Wang, T. Maiyalagan and X. Wang, Review on Recent Progress in Nitrogen-Doped Graphene: Synthesis, Characterization, and Its Potential Applications, *ACS Catal.*, 2012, **2**, 781–794.
6 M. Takase, T. Narita, W. Fujita, M. S. Asano, T. Nishinaga, H. Benten, K. Yoza and K. Müllen, Pyrrole-Fused Azacoronene Family: The Influence of Replacement with Dialkoxybenzenes on the Optical and Electronic Properties in Neutral and Oxidized States, *J. Am. Chem. Soc.*, 2013, **135**, 8031–8040.
7 X.-Y. Wang, M. Richter, Y. He, J. Björk, A. Riss, R. Rajesh, M. Garnica, F. Hennersdorf, J. J. Weigand, A. Narita, R. Berger, X. Feng, W. Auwärter, J. V. Barth, C.-A. Palma and K. Müllen, Exploration of pyrazine-embedded antiaromatic polycyclic hydrocarbons generated by solution and on-surface azomethine ylide homocoupling, *Nat. Commun.*, 2017, **8**, 1948.
8 J. E. Anthony, J. S. Brooks, D. L. Eaton and S. R. Parkin, Functionalized Pentacene: Improved Electronic Properties from Control of Solid-State Order, *J. Am. Chem. Soc.*, 2001, **123**, 9482–9483.
9 C. D. Sheraw, T. N. Jackson, D. L. Eaton and J. E. Anthony, Functionalized Pentacene Active Layer Organic Thin-Film Transistors, *Adv. Mater.*, 2003, **15**, 2009–2011.
10 M. Chu, J.-X. Fan, S. Yang, D. Liu, C. F. Ng, H. Dong, A.-M. Ren and Q. Miao, Halogenated Tetraazapentacenes with Electron Mobility as High as 27.8 $cm^2 V^{-1} s^{-1}$ in Solution-Processed n-Channel Organic Thin-Film Transistors, *Adv. Mater.*, 2018, **30**, 1803467.
11 K. Takimiya, K. Bulgarevich, M. Abbas, S. Horiuchi, T. Ogaki, K. Kawabata and A. Ablat, ''Manipulation'' of Crystal Structure by Methylthiolation Enabling Ultrahigh Mobility in a Pyrene-Based Molecular Semiconductor, *Adv. Mater.*, 2021, **33**, 2102914.

12 K. Takimiya, K. Bulgarevich and K. Kawabata, Crystal-Structure Control of Molecular Semiconductors by Methylthiolation: Toward Ultrahigh Mobility, *Acc. Chem. Res.*, 2024, **57**, 884–894.

13 K. Takimiya, K. Bulgarevich and S. Horiuchi, Contrasted behaviours of methylthiolated perylene and pyrene as organic semiconductors: implications of molecular electronic structure and crystal structure, *J. Mater. Chem. C*, 2023, **11**, 10809–10815.

14 K. Bulgarevich, S. Horiuchi, T. Ogaki and K. Takimiya, 1,3,6,8-Tetrakis(methylchalcogeno)pyrenes: Effects of Chalcogen Atoms on the Crystal Structure and Transport Properties, *Chem. Mater.*, 2022, **34**, 6606–6616.

15 P. Pal, K. Bulgarevich, R. Hanaki, K. Kawabata and K. Takimiya, Extension of the π-conjugated core of methylchalcogenolated polycyclic aromatic hydrocarbons: synthesis and characterization of 1,4,7,10-tetrakis(methylthio)- and tetramethoxy-coronene, *Chem. Sci.*, 2025, **16**, 15368–15377.

16 K. Takimiya, K. Sahara, M. Inoue, K. Bulgarevich and K. Kawabata, Isoelectronic Substitution of a High-performance Organic Semiconductor with Selenium Atoms: Synthesis and Characterization of Methylthiolated Dibenzo[*cd*,*gh*][2,5]diselenapentalene, *Asian J. Org. Chem.*, 2025, **14**, e202500173.

17 K. Bulgarevich and K. Takimiya, What makes brickwork crystal structures favourable? A case study on methylthiolated arenes and heteroarenes for high-mobility molecular semiconductors, *CrystEngComm*, 2025, **27**, 4776–4786.

18 K. Bulgarevich, S. Horiuchi and K. Takimiya, Crystal-Structure Simulation of Methylthiolated Peri-Condensed Polycyclic Aromatic Hydrocarbons for Identifying Promising Molecular Semiconductors: Discovery of 1,3,8,10-tetrakis(methylthio)peropyrene Showing Ultrahigh Mobility, *Adv. Mater.*, 2023, **35**, 2305548.

19 T. Nakazato, T. Kamatsuka, J. Inoue, T. Sakurai, S. Seki, H. Shinokubo and Y. Miyake, The reductive aromatization of naphthalene diimide: a versatile platform for 2,7-diazapyrenes, *Chem. Commun.*, 2018, **54**, 5177–5180.

20 T. Nakazato, W. Matsuda, T. Sakurai, S. Seki, H. Shinokubo and Y. Miyake, Synthesis and Crystal Packing Structures of 2,7-Diazapyrenes with Various Alkyl Groups at 1,3,6,8-Positions, *Chem. Lett.*, 2020, **49**, 465–468.

21 X. Ye, Y. Liu, Q. Han, C. Ge, S. Cui, L. Zhang, X. Zheng, G. Liu, J. Liu, D. Liu and X. Tao, Microspacing In-Air Sublimation Growth of Organic Crystals, *Chem. Mater.*, 2018, **30**, 412–420.

22 G. Sheldrick, SHELXT – Integrated space-group and crystal-structure determination, *Acta Crystallogr., Sect. A: Found. Adv.*, 2015, **71**, 3–8.

23 G. Sheldrick, Crystal structure refinement with SHELXL, *Acta Crystallogr., Sect. C: Struct. Chem.*, 2015, **71**, 3–8.

24 O. V. Dolomanov, L. J. Bourhis, R. J. Gildea, J. A. K. Howard and H. Puschmann, OLEX2: a complete structure solution, refinement and analysis program, *J. Appl. Crystallogr.*, 2009, **42**, 339–341.

25 K. Bulgarevich, K. Sakamoto, T. Yasuda, T. Minari and M. Takeuchi, Operational Stability Enhancement of Polymeric Organic Field-Effect Transistors by Amorphous Perfluoropolymers Chemically Anchored to Gate Dielectric Surfaces, *Adv. Electron. Mater.*, 2020, **6**, 2000161.

26 M. J. Frisch, G. W. Trucks, H. B. Schlegel, G. E. Scuseria, M. A. Robb, J. R. Cheeseman, G. Scalmani, V. Barone, G. A. Petersson, H. Nakatsuji, X. Li, M. Caricato, A. V. Marenich, J. Bloino, B. G. Janesko, R. Gomperts, B. Mennucci, H. P. Hratchian, J. V. Ortiz, A. F. Izmaylov, J. L. Sonnenberg, D. Williams-Young, F. Ding, F. Lipparini, F. Egidi, J. Goings, B. Peng, A. Petrone, T. Henderson, D. Ranasinghe, V. G. Zakrzewski, J. Gao, N. Rega, G. Zheng, W. Liang, M. Hada, M. Ehara, K. Toyota, R. Fukuda, J. Hasegawa, M. Ishida, T. Nakajima, Y. Honda, O. Kitao, H. Nakai, T. Vreven, K. Throssell, J. A. Montgomery Jr., J. E. Peralta, F. Ogliaro, M. J. Bearpark, J. J. Heyd, E. N. Brothers, K. N. Kudin, V. N. Staroverov, T. A. Keith, R. Kobayashi, J. Normand, K. Raghavachari, A. P. Rendell, J. C. Burant, S. S. Iyengar, J. Tomasi, M. Cossi, J. M. Millam, M. Klene, C. Adamo, R. Cammi, J. W. Ochterski, R. L. Martin, K. Morokuma, O. Farkas, J. B. Foresman and D. J. Fox, *Gaussian 16 Rev. C.02.*, 2016.

27 E. J. Baerends, N. F. Aguirre, N. D. Austin, J. Autschbach, F. M. Bickelhaupt, R. Bulo, C. Cappelli, A. C. T. van Duin, F. Egidi, C. Fonseca Guerra, A. Förster, M. Franchini, T. P. M. Goumans, T. Heine, M. Hellström, C. R. Jacob, L. Jensen, M. Krykunov, E. van Lenthe, A. Michalak, M. M. Mitoraj, J. Neugebauer, V. P. Nicu, P. Philipsen, H. Ramanantoanina, R. Rüger, G. Schreckenbach, M. Stener, M. Swart, J. M. Thijssen, T. Trnka, L. Visscher, A. Yakovlev and S. van Gisbergen, The Amsterdam Modeling Suite, *J. Chem. Phys.*, 2025, **162**, 162501.

28 S.-H. Wen, A. Li, J. Song, W.-Q. Deng, K.-L. Han and W. A. Goddard, III, First-Principles Investigation of Anistropic Hole Mobilities in Organic Semiconductors, *J. Phys. Chem. B*, 2009, **113**, 8813–8819.

29 S. Werner, T. Vollgraff, Q. Fan, K. Bania, J. M. Gottfried and J. Sundermeyer, Reductive O-triflylation of naphthalene diimide: access to alkyne- and amine-functionalized 2,7-diazapyrenes, *Org. Chem. Front.*, 2021, **8**, 5013–5023.

30 A. Mukherjee, A. A. Akulov, S. Santra, M. V. Varaksin, G. A. Kim, D. S. Kopchuk, O. S. Taniya, G. V. Zyryanov and O. N. Chupakhin, 2,7-Diazapyrenes: a brief review on synthetic strategies and application opportunities, *RSC Adv.*, 2022, **12**, 9323–9341.

31 L. Meerpoel and G. Hoornaert, Synthesis of 3,5-dihalogeno-2*H*-1,4-oxazin-2-ones from cyanohydrines, *Tetrahedron Lett.*, 1989, **30**, 3183–3186.

32 S. Vanlaer, W. M. De Borggraeve, A. Voet, C. Gielens, M. De Maeyer and F. Compernolle, Spirocyclic Pyridoazepine Analogues of Galanthamine: Synthesis, Modelling Studies and Evaluation as Inhibitors of Acetylcholinesterase, *Eur. J. Org. Chem.*, 2008, 2571–2581.

33 M. Gingras and F. Dubois, Synthesis of carbohelicenes and derivatives by ''carbenoid couplings'', *Tetrahedron Lett.*, 1999, **40**, 1309–1312.
34 F. B. Mallory and C. W. Mallory, *Organic Reactions*, John Wiley and Sons, 1984.
35 K. Bulgarevich and K. Takimiya, Crystal-structure simulation of molecular semiconductors: brickwork-related crystal structures of methylthiolated peri-condensed polycyclic aromatic hydrocarbons, *Mater. Horiz.*, 2023, **10**, 5492–5499.
36 C. A. Hunter and J. K. M. Sanders, The nature of. π–π interactions, *J. Am. Chem. Soc.*, 1990, **112**, 5525–5534.
37 J. H. Williams, The molecular electric quadrupole moment and solid-state architecture, *Acc. Chem. Res.*, 1993, **26**, 593–598.
38 T. Mori, Quadrupole moments determine the crystal structures of organic semiconductors, *J. Mater. Chem. C*, 2025, **13**, 17078–17093.
39 T. Mori, Crystal structures of organic semiconductors, *Bull. Chem. Soc. Jpn.*, 2025, **98**, uoaf109.
40 (*a*) CCDC 2528768: Experimental Crystal Structure Determination, 2026, DOI: 10.5517/ccdc.csd.cc2qwd56; (*b*) CCDC 2528769: Experimental Crystal Structure Determination, 2026, DOI: 10.5517/ccdc.csd.cc2qwd67; (*c*) CCDC 2528770: Experimental Crystal Structure Determination, 2026, DOI: 10.5517/ccdc.csd.cc2qwd78; (*d*) CCDC 2528771: Experimental Crystal Structure Determination, 2026, DOI: 10.5517/ccdc.csd.cc2qwd89; (*e*) CCDC 2528772: Experimental Crystal Structure Determination, 2026, DOI: 10.5517/ccdc.csd.cc2qwd9b; (*f*) CCDC 2528773: Experimental Crystal Structure Determination, 2026, DOI: 10.5517/ccdc.csd.cc2qwdbc; (*g*) CCDC 2528774: Experimental Crystal Structure Determination, 2026, DOI: 10.5517/ccdc.csd.cc2qwdcd; (*h*) CCDC 2528775: Experimental Crystal Structure Determination, 2026, DOI: 10.5517/ccdc.csd.cc2qwddf; (*i*) CCDC 2528776: Experimental Crystal Structure Determination, 2026, DOI: 10.5517/ccdc.csd.cc2qwdfg; (*j*) CCDC 2528777: Experimental Crystal Structure Determination, 2026, DOI: 10.5517/ccdc.csd.cc2qwdgh; (*k*) CCDC 2528778: Experimental Crystal Structure Determination, 2026, DOI: 10.5517/ccdc.csd.cc2qwdhj.